Theoretical investigation of the pure and Zn-doped α and δ phases of Bi_2O_3

Johan M. Carlsson* and Bo Hellsing
Experimental Physics, School of Physics and Engineering Physics, Chalmers University of Technology and Göteborg University, SE-412 96 Gothenburg, Sweden

Helder S. Domingos and Paul D. Bristowe
Department of Materials Science and Metallurgy, University of Cambridge, Pembroke Street, Cambridge CB2 3QZ, United Kingdom
(Received 13 December 2001; published 20 May 2002)

We have studied the atomic and electronic structure of pure and Zn-doped α and δ phases of Bi_2O_3 by *first-principles* calculations. For the pure α phase which is monoclinic, good agreement was obtained between the experimental and calculated structural parameters and, in addition, the calculated density of states in the valence band and the optical band gap correlated well with photoemission spectra. For the pure δ phase, which has a defective fluorite structure, the calculations suggest that of three possible oxygen vacancy structures, $\langle 100\rangle$-vacancy ordering is preferred. This phase, however, must be considered as a supercooled phase at $T=0$ K since we found that a single displaced vacancy (i.e., one that deviates from $\langle 100\rangle$ ordering) can trigger a δ-α phase transition. Similarly, a Zn substitutional impurity in the δ phase can also trigger this phase transition. The formation energy of a Zn impurity in the α phase was found to be 1.34 eV, resulting in a maximum impurity concentration of 7.1×10^{-6} at. % Zn at $T=1000$ K. The low solubility of Zn in the α phase of Bi_2O_3 is consistent with the observed phase separation between ZnO and Bi_2O_3.

DOI: 10.1103/PhysRevB.65.205122 PACS number(s): 71.20.−b, 61.72.Ss, 71.55.−i, 84.32.Ff

I. INTRODUCTION

Bismuth oxide (Bi_2O_3) is an electroceramic material with a wide range of applications. Bi_2O_3 doped with potassium exhibits superconductivity[1] and codoping with barium increases the critical temperature (T_c) to 31 K which was the highest observed T_c value for noncuprate superconductors[2] at the time. The high-temperature δ phase of Bi_2O_3 shows an exceptionally high ionic conductivity at temperatures above the phase transition temperature.[3] The δ phase can be stabilized by rare-earth metal doping to maintain its cubic structure at room temperature and in this form it has been used as a solid electrolyte.

Bi_2O_3 is also one of the most important additives in the production of ZnO varistors[4] where the Bi content has a fundamental influence on the nonlinear *I-V* characteristics of the devices.[5] It is frequently observed that the majority of the Bi atoms in varistor materials form more or less pure Bi_2O_3 phases at the triple junctions between the ZnO grains.[6,7] The Bi concentration inside the ZnO grains is very low[8] but a small amount of Bi can leak out of the triple-junction phases to decorate the grain boundaries in the host material.[9] The Bi accumulation in the grain boundaries is consistent with our recent theoretical investigation of the Bi doping of ZnO, where we found that it was energetically favorable for Bi atoms to segregate to a $\Sigma=13$ [001] tilt grain boundary.[10] The reason why Bi_2O_3 phases form at triple junctions and their inability to dissolve Zn is not as well understood and needs to be further investigated.

In its pure form Bi_2O_3 has four known phases.[11–14] The monoclinic α phase is the stable, low-temperature phase. The structure of the α phase was first determined by Sillén[11] and later studies[12–14] have refined the atomic positions slightly. The electronic structure of the α phase has been investigated using photoemission experiments,[15] X-α cluster calculations,[16] and self-consistent–complete neglect of differential overlap (SC-CNDO) (Ref. 17) and linear muffin-tin orbital (LMTO) calculations.[18]

At 730 °C, Bi_2O_3 transforms into the cubic high-temperature δ phase. There is agreement that the δ phase has a defective fluorite (CaF_2) structure, in which the Bi atoms occupy the fcc sites, but there has been debate regarding the oxygen sublattice.[11,13,14,19,20] Sillén proposed an ordered structure with two oxygen vacancies per unit cell aligned along the $\langle 111\rangle$ directions.[11] Gattow and Schröder suggested a fractional occupancy of 3/4 for each of the eight oxygen sites in the fluorite structure[19] while Harwig extended the number of possible sites by including the interstitial positions.[13] Neutron diffraction experiments indicated a more complicated vacancy structure in which the oxygen atoms also deviated from their ideal sites in the fluorite structure.[20] Battle *et al.* later suggested that $\langle 110\rangle$-vacancy ordering may be more favorable in the pure δ phase while $\langle 111\rangle$ ordering is favorable if the δ phase is stabilized by rare-earth metal doping.[21] LMTO calculations[22] have favored $\langle 111\rangle$-vacancy ordering along the lines of the Sillén model but rigid-ion model calculations[23,24] showed that the system could gain energy by breaking the long-range $\langle 111\rangle$-vacancy order by introducing local $\langle 110\rangle$- or $\langle 100\rangle$-ordered vacancy structures. However, no one has made a systematic study of how the heat of formation ΔH, varies when an O atom is moved in between the sites in the oxygen sublattice to form the three possible ordered vacancy structures. This process is also of interest for understanding the mechanism behind the high ionic conductivity of the δ phase. Boyapati *et al.*[25] have recently proposed a possible path for the O atoms which involves interstitial sites, but it is beyond the scope of this article to investigate all available conduction paths.

The α phase has a wide band gap[15] but the situation in the δ phase is less clear. The band structure calculated by the LMTO method[22] indicated that the δ phase is metallic but SC-CNDO calculations gave a considerable band gap.[17] Measurements of the conductivity in thin Bi_2O_3 films have

shown that there is a finite density of states at the Fermi level.[26]

A tetragonal β phase or a bcc γ phase may occur upon cooling of the δ phase below 730 °C before the material finally transforms into the α phase. Recently, a fifth hexagonal high-pressure phase has been discovered when the α phase is heated under pressure.[27,28]

In this article, we have investigated the atomic and electronic structure of the α and δ phases of Bi_2O_3 by *first-principles* calculations which were performed in a supercell geometry using the serial and parallel versions of the computer code DACAPO.[29] We have determined the equilibrium atomic structure of the α phase and also calculated its band structure and electronic density of states. The most favorable vacancy ordering for the oxygen sublattice in the unit cell of the δ phase has been determined and the corresponding band structure is presented. The stability of the δ phase and the possibility of treating a high-temperature phase in a $T=0$ K calculation is further discussed. The effect of doping Bi_2O_3 with Zn atoms was also studied to get some understanding of the phase separation between Bi_2O_3 and ZnO observed in varistor materials.

II. COMPUTATIONAL DETAILS

The total energy calculations in this study were based on density functional theory[30,31] (DFT) using the PW-91 version of the generalized gradient approximation[32] (GGA) for the exchange-correlation functional. The wave functions were expanded in a plane-wave basis set with a kinetic energy cutoff set to 400 eV. This gives a total energy that is converged to within 60 meV/(Bi_2O_3 molecule). The ultrasoft pseudopotentials[33] for O, Zn, and Bi were generated from a scalar-relativistic all-electron calculation to achieve a good description of the core electrons for the Bi atom. The semicore electrons, $2s$ for O, $3d$ for Zn, and $5d$ for Bi, were treated as valence electrons to obtain as good a description of the bonding in the crystal as possible and to keep a consistent number of valence electrons in the substitution process. The Brillouin zone of the supercell was sampled according to the Monkhorst-Pack scheme.[34] A $(2\times2\times2)$ grid was used for the α phase and a $(3\times3\times3)$ grid was used for the δ phase. This gives a total energy which is converged to within 25 meV/(Bi_2O_3 molecule). A finite-temperature smearing of $kT=0.01$ eV was applied to improve the convergence.[35]

The unit cell of the α phase contains four Bi_2O_3 molecules while the unit cell for the cubic δ phase contains two Bi_2O_3 molecules. The large supercells used to describe dilute Zn doping in the α and δ phases were composed of four and eight unit cells of each structure, respectively. Thus, in each case, the supercells contained 80 atoms. Eight unit cells were also used to study the interactions between oxygen vacancies in the δ phase. The equilibrium lattice parameters were determined by varying the cell vectors independently and finding the minimum in the total energy of the supercell. The atomic positions were relaxed by a preconditioned BFGS algorithm until the average forces on the atoms were less than 0.01 eV/Å. The total density of states (DOS) shown in Figs. 1 and 4 was calculated by applying a Gaussian smearing of 0.1 eV to the eigenvalues. The projected density of states (PDOS) was obtained by projecting the wave functions onto the atomic wave functions of the pseudopotentials. The band structures of the α and δ phases of Bi_2O_3 were obtained by calculating the Kohn-Sham eigenvalues for 40 and 60 k points along the irreducible wedge of the Brillouin zone.

III. FORMALISM TO CALCULATE THE IMPURITY CONCENTRATION

The formalism used to determine the equilibrium concentration of Zn impurities in Bi_2O_3 is based on the articles by Zhang and Northrup[36] and Van de Walle *et al.*[37] The equilibrium concentration C_i of an impurity is described by

$$C_i(E_{form},T)=N_s e^{-E_{form}/k_BT}, \tag{1}$$

where E_{form} is the formation energy of the impurity and N_s is the number of available sites for the impurity to occupy. In the present case, where we consider Zn substitution for Bi, this would be the number of Bi sites per unit volume. The formation energy is the change in Gibbs free energy due to the inclusion of the impurity in the system. We have used the DFT method to calculate the total energy of the impurity system for the α and δ phases of Bi_2O_3. The formation energy E_{form} for the Zn impurity was then obtained as

$$E_{form}=E_{Bi_2O_3:Zn}-E_{Bi_2O_3}+\mu_{Bi}-\mu_{Zn}-n_e\mu_e, \tag{2}$$

where $E_{Bi_2O_3}$ and $E_{Bi_2O_3:Zn}$ denote the total energy of the supercell for pure and Zn-doped Bi_2O_3. μ_{Bi} and μ_{Zn} refer to the chemical potentials of the Bi and Zn reservoirs, respectively. n_e is the additional number of electrons at the impurity, taken from the electron reservoir μ_e, which changes the charge of the impurity from its intrinsic charge state. We have, however, only considered the intrinsic charge state of the Zn impurity in Bi_2O_3 and thus the last term in Eq. (2) is absent since no additional electrons have been added or removed from the Zn atom.

The formation energy in Eq. (2) for Zn substitution in Bi_2O_3 is dependent on the chemical potentials of the Zn and Bi atoms and μ_{Zn} and μ_{Bi} need to be considered as variables. The chemical potential of an atom in a metal oxide is, however, not well defined since only the chemical potential of the smallest stoichiometric molecular unit can be determined. The chemical potential for the individual atoms are therefore free to vary under the restriction that their sum gives the value for the molecular unit. The chemical potentials are dependent on the chemical environment in the system and the upper limit is set by the value in the bulk metal since a higher value would favor the formation of a metallic phase in the system. The lower bound is set by the heat of formation, ΔH, for the compound since the constituents can at most gain the formation energy of the compound.

ZnO and Bi_2O_3 are two of the most common compounds in a varistor material. Bi_2O_3 was therefore considered as the reservoir for the extracted Bi atoms since we expect that there are enough vacancies and oxygen atoms available at the temperatures considered to incorporate the Bi atoms into

TABLE I. The chemical potentials (μ) for the pure substances and the heats of formation (ΔH) used to calculate the formation energy of a Zn impurity in the α and δ phases of Bi_2O_3 using Eq. (2).

$\mu_O^{O_2}$ [eV]	μ_{Bi}^{bulk} [eV]	μ_{Zn}^{bulk} [eV]	ΔH_{ZnO} [eV]	$\Delta H_{\alpha\text{-}Bi_2O_3}$ [eV]	$\Delta H_{\delta\text{-}Bi_2O_3}$ [eV]
−436.5	−1969.1	−1731.4	−3.08	−6.34	−5.56

an at least Bi_2O_3-like environment. The relationship between the chemical potentials in Bi_2O_3 is given by

$$\mu_{Bi_2O_3}=2\mu_{Bi}+3\mu_O=2\mu_{Bi}^{bulk}+3\mu_O^{O_2}+\Delta H_{Bi_2O_3}. \quad (3)$$

The lower limit on μ_{Bi} corresponds to an oxygen-rich environment such that $\mu_O=\mu_O^{O_2}$, giving the limits for μ_{Bi} as

$$\mu_{Bi}^{Bulk}+\frac{\Delta H_{Bi_2O_3}}{2}<\mu_{Bi}<\mu_{Bi}^{bulk}. \quad (4)$$

The reservoir for Zn is ZnO which sets an upper limit for μ_{Zn} from the relationship between the chemical potentials in ZnO:

$$\mu_{ZnO}=\mu_{Zn}+\mu_O=\mu_{Zn}^{bulk}+\mu_O^{O_2}+\Delta H_{ZnO}. \quad (5)$$

μ_O is, however, constant throughout the system which means that μ_{Zn} and μ_{Bi} are coupled through μ_O. This gives the limiting ZnO line which is shown bold in Fig. 6 as described later:

$$\mu_{Bi}(\mu_{Zn})=\mu_{Bi}^{bulk}+\frac{1}{2}(\Delta H_{Bi_2O_3}-3\Delta H_{ZnO}-3\mu_{Zn}^{bulk})+\frac{3\mu_{Zn}}{2}. \quad (6)$$

The calculated chemical potentials of the pure elements and the heats of formation for ZnO and the α and δ phases of Bi_2O_3 are given in Table I.

IV. RESULTS

In the first two sections we present our results for the atomic and electronic structures of the pure α and δ phases. In Sec. IV C we describe the effect of doping the α and δ phases with Zn impurities.

A. α phase of Bi_2O_3

To obtain the equilibrium lattice parameters of the monoclinic α phase we used the atomic fractional coordinates determined by Malmros[12] and varied the lattice parameters a, b, c and the angle β independently while computing the energy. The lowest-energy configuration resulted in the parameters given in Table II which were close to the experimental data.[11–13] The calculated unit cell volume was 1.5% larger than the experimental value which is common for DFT calculations using the GGA exchange-correlation functional. The forces on the atoms in the equilibrium unit cell were small (<0.15 eV/Å) and the relaxation simply resulted in small adjustments to the positions. The optimized atomic positions are given in Table III and they were not only in agreement with the Malmros positions[12] but also with the values reported by Harwig[13] which are also given for comparison.

Bi_2O_3 is an ionic material which exhibits considerable charge transfer from the Bi atoms to the O atoms. The electrons are to a large extent localized around the atoms with only a small amount of delocalized charge. The charge localization was reflected in the flat dispersion of the bands in Fig. 1 and the DOS had a distinct peak structure related to the atomic contributions from the individual Bi and O atoms. The center of gravity for the semicore electrons, $5d$ in Bi and $2s$ in O, was located at -23.5 eV and -18 eV below the Fermi level. The $6s$ band from bismuth was divided into two peaks centered around -11 eV and -9.6 eV. Debies and Rabalais[15] attributed the upper of these two peaks to O $2p$ electrons but the calculated PDOS revealed that both peaks had Bi $6s$ character and that they overlapped slightly with the $2s$ and $2p$ orbitals from neighboring O atoms in agreement with interpretations from previous calculations.[17,18] The main amplitude of the oxygen $2p$ states was instead located in the valence band which consequently had strong p character and its center of gravity was located at -3.7 eV. The amount of occupied Bi $6p$ states in the valence band was limited due to the charge transfer of a fraction of the $6p$ electrons from the bismuth atoms to the oxygen atoms and most of the Bi $6p$ states were located in the conduction band. The PDOS for Bi atoms showed, in addition, a $6s$ peak from the Bi atoms just below the maximum of the valence band.

Comparing the calculated DOS to photoemission spectra[15] results in fairly good correspondence particularly for the valence band. Debies and Rabalais[15] reported the center of gravity for the Bi $6s$ band at -12.4 eV, -10.5 eV for the O $2p$, and -3.5 eV for the Bi $6p$ band. The calculated peaks for the semicore electrons were slightly shifted towards higher energies compared to the experimental peaks which were located at -28.8 eV and -25.7 eV for Bi $5d_{3/2}$ and $5d_{5/2}$ and -21 eV for the O $2s$ band. These shifts are possibly due to the use of pseudopotentials which are not accurately describing of the electron-ion interaction for these semicore electrons. An incorrect treatment of the correlation effects for the d electrons can also contribute to the upward shift for the $5d$ electrons.

The α phase has an indirect band gap since both the valence band and the conduction band have minima at the Γ point. The valence-band maximum occurs at the zone boundary in the [100] direction. This gives an indirect band gap of 2.6 eV and an energy gap of 2.7 eV at the Γ point. These calculated values were in much better agreement with the experimental result $E_g^{expt}=2.5$ eV,[15] compared to previous calculations which have either overestimated the magnitude of the band gap, $E_g=6.2$ eV,[17] or underestimated the band gap, $E_g=1.68$ eV.[18] We believe that the good description of the band gap in the α phase is connected to the ionic character of the material and the fact that the valence and conduction bands are composed of s and p electrons where the

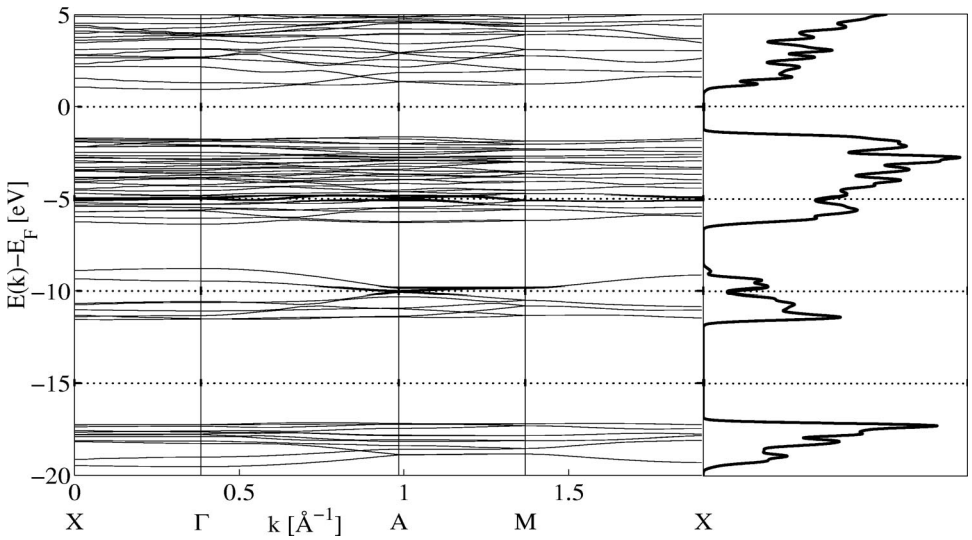

FIG. 1. The band structure and DOS for α-Bi_2O_3. The lowest-energy peak originates from the O $2s$ electrons, the double peak at -10 eV comes from the Bi $6s$ electrons, and the valence band has a strong O $2p$ character.

correlation effects are not as severe as for d electrons. Other ionic s-p bonded metal oxides such as the α and κ phases of Al_2O_3 (Ref. 38) also give reasonable values for the band gap. However, in ZnO where the d electrons are close to the valence band, correlation effects result in an underestimated band gap compared to experiments.[39,40]

B. δ phase of Bi_2O_3

The δ phase of Bi_2O_3 has a defective CaF_2 structure[11,13,14,19–21] as shown in Fig. 2. The Bi atoms form a fcc lattice but only six oxygen atoms are present in the unit cell due to the stoichiometry of Bi_2O_3. The eight sites in the cubic oxygen sublattice would then have either two vacancies[11,14] or be fractionally occupied.[19] An even larger number of sites are available if deviations from the ideal positions in the sublattice are allowed.[13] The supercell method is, however, restricted to periodic systems and long-range disorder cannot be modeled accurately. We have, therefore, considered just the three possible ordered vacancy configurations in the oxygen sublattice to find the optimal vacancy ordering in the δ phase and subsequently performed relaxations to determine deviations from the ideal sites. The three vacancy orientations correspond to aligning the two vacancies along the space diagonal $\langle 111\rangle$, along the plane diagonal $\langle 110\rangle$, or along an unit cell axis $\langle 100\rangle$. The unit cell of the δ phase in the $\langle 111\rangle$- and $\langle 100\rangle$-vacancy configurations is shown in Fig. 2.

We have, in addition, mapped out the heat of formation of the δ phase for configurations intermediate between the $\langle 111\rangle$- and $\langle 100\rangle$-vacancy structures by displacing an O atom along the edge of the sublattice as indicated by the arrows in Fig. 2. The purpose of these calculations was to determine whether there are barriers for oxygen diffusion between the different structures. The values for the heat of formation shown in Fig. 3 were computed using the same size supercell and the atoms were held fixed without relaxation. The optimal lattice parameters for unit cells of the three different ordered vacancy structures were subsequently determined independently and the atoms were relaxed to determine the total difference in the heat of formation between the three configurations. The relaxation energy per Bi_2O_3 molecule for the $\langle 110\rangle$- and $\langle 100\rangle$-vacancy configurations is indicated by the arrows in Fig. 3. The symmetry of the $\langle 111\rangle$-vacancy structure resulted in negligible forces on the atoms in the cell which is why no relaxation occurred for this structure.

Figure 3 shows that the $\langle 111\rangle$-vacancy structure is metastable although it possesses high symmetry. Despite the fact that there were no forces on the atoms in the perfect $\langle 111\rangle$-vacancy cell, there was no energy barrier for the dis-

TABLE II. The experimental and calculated lattice parameters in the α and δ phases of Bi_2O_3. β is the angle between the a and c axes.

Phase	a	b	c	β	Ref.
α	5.83	8.14	7.48	67.07°	11
	5.8486	8.1661	7.5097	113°	12
	5.8496	8.1648	7.5101	112.977°	13
	5.920	8.182	7.492	112.6°	This work
δ	5.525	-	-	90°	11
	5.6595	-	-	90°	13
	5.648	-	-	90°	20
	5.546	-	-	90°	This work

TABLE III. The unit cell contents of α-Bi_2O_3 given in fractional coordinates along the a, b, and c axes. The three left columns present the results of this work while the three right columns are the values reported by Harwig (Ref. 13).

	This work			Ref. 13		
Atom	x	y	z	x	y	z
Bi_1	0.5242	0.1840	0.3645	0.5242	0.1843	0.3615
Bi_2	0.0393	0.0421	0.7768	0.0404	0.0425	0.7767
O_1	0.7762	0.2999	0.7060	0.7783	0.3037	0.7080
O_2	0.2340	0.0507	0.1249	0.2337	0.0467	0.1266
O_3	0.2702	0.0314	0.5119	0.2658	0.0294	0.5115

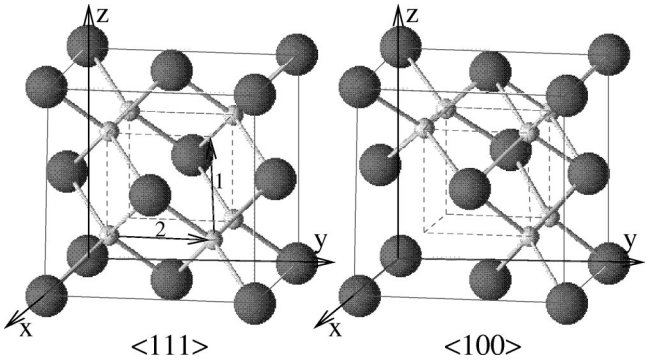

FIG. 2. The unit cell for the defective fluorite structure of δ-Bi_2O_3. The Bi atoms are dark gray and form a fcc lattice while the white O atoms occupy the corners in the cubic sublattice indicated by the dashed gray lines. The $\langle 111\rangle$- and $\langle 100\rangle$-oxygen-vacancy structures are shown and the arrows indicate how the displacement of an oxygen atom can transform one structure into the other, passing the through the $\langle 110\rangle$ configuration.

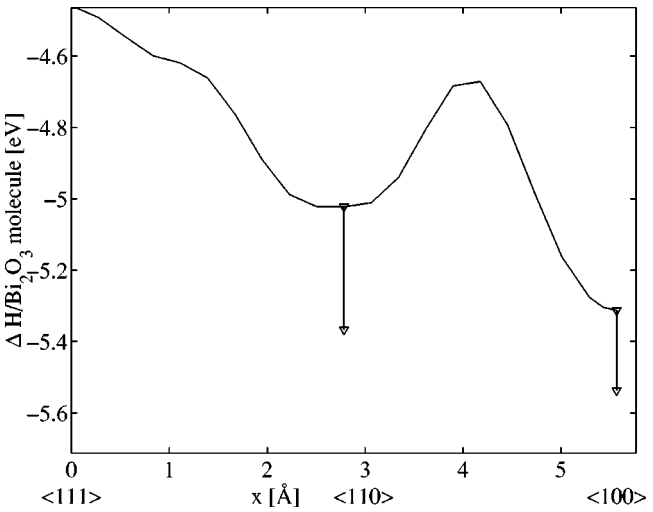

FIG. 3. The variation of ΔH (unrelaxed) per Bi_2O_3 molecule as a function of different crystallographically ordered oxygen vacancy structures in δ-Bi_2O_3. The vertical arrows indicate the relaxation energy for the $\langle 110\rangle$- and $\langle 100\rangle$-vacancy configurations.

placement an O atom out of its ideal site. The forces on the displaced atom were not pointing back towards its original position but instead towards the $\langle 110\rangle$-vacancy configuration. The $\langle 110\rangle$-vacancy structure was found to be a local minimum with an energy gain of 0.56 eV per Bi_2O_3 molecule compared to the $\langle 111\rangle$-vacancy configuration. After relaxation the energy gain increased to 0.9 eV per Bi_2O_3 molecule. There was a barrier for displacing an O atom out of its ideal site in the $\langle 110\rangle$-vacancy configuration. The barrier for transformation into the $\langle 100\rangle$-vacancy structure had an energy of 0.35 eV per Bi_2O_3 molecule and the peak was located at the interstitial position midway between the corners. The heat of formation increased in transforming from $\langle 110\rangle$- to $\langle 100\rangle$-vacancy ordering and the energy difference was 0.39 eV before relaxation and 0.17 eV per Bi_2O_3 molecule after relaxation. This means that the $\langle 100\rangle$-vacancy structure was the energetically most favorable configuration and the total energy difference between the $\langle 111\rangle$- and $\langle 100\rangle$-vacancy structures amounted to 1.1 eV per Bi_2O_3 molecule after relaxation. These results stand in contrast to previous LMTO calculations which favored the $\langle 111\rangle$-vacancy ordered structure.[22]

The optimal lattice parameter for the $\langle 100\rangle$-vacancy ordered δ phase was 5.546 Å (see Table II). This value is close to Sillén's value of $a=5.52$ Å,[11] but slightly smaller than Harwig's value of $a=5.66$ Å.[13] The optimized atomic positions for the δ phase in Table IV show that the relaxation of the atoms in the $\langle 100\rangle$-vacancy-ordered cell displaced the Bi atoms away from the line of O vacancies and reduced the Bi-O bond length to 2.1, 2.1, and 2.2 Å for the three nearest-neighboring O atoms. This deviation of the Bi atoms from their ideal sites in the fluorite structure is not large enough for them to occupy interstitial sites as has been proposed previously,[13,20,21] but it indicates that the Bi_2O_3 crystal is in this way trying to minimize the energy by moving the Bi atoms closer to the O atoms, leaving large empty channels through the crystal.

Figure 4 compares the computed DOS for the $\langle 100\rangle$- and $\langle 111\rangle$-vacancy structures in the δ phase where it is seen that there is a general trend for occupied states in the $\langle 111\rangle$ structure to shift towards lower energies in the $\langle 100\rangle$ structure. The PDOS shows that these states reside on the two O atoms in the unit cell which are farthest from the O vacancies. These O atoms experience four nearest-neighbor Bi atoms and six next-nearest-neighbor O atoms. The other four O atoms have four nearest-neighbor Bi atoms and four next-nearest-neighbor O atoms. In the $\langle 111\rangle$-vacancy structure all O atoms experience the same environment with four nearest-neighbor Bi atoms and four next-neighbor O atoms, and the peaks in the DOS are more narrow.

The perfect [100]-vacancy ordering for the δ phase introduces an anisotropy into the Bi_2O_3 lattice since the periodicity along the [100] direction is half the periodicity in the [010] and [001] direction. This is reflected in the band structure for the [100]-ordered structure at the X point in Fig. 4. There is a zone boundary at the X point in the k_y direction but not in the k_x direction. This gives band gaps for bands which pass through the X point while there are no corresponding band gaps at the X' point.

TABLE IV. The unit cell contents of $\langle 100\rangle$-vacancy-ordered δ-Bi_2O_3 given in fractional coordinates along the *a*, *b*, and *c* axes.

Atom	*x*	*y*	*z*
Bi_1	0	0	0
Bi_2	0.5	0.5298	0
Bi_3	0.5	0	0.5298
Bi_4	0	0.5297	0.5297
O_1	0.25	0.7647	0.2647
O_2	0.75	0.7647	0.2647
O_3	0.25	0.2647	0.7647
O_4	0.75	0.2647	0.7647
O_5	0.25	0.7647	0.7647
O_6	0.75	0.7647	0.7647

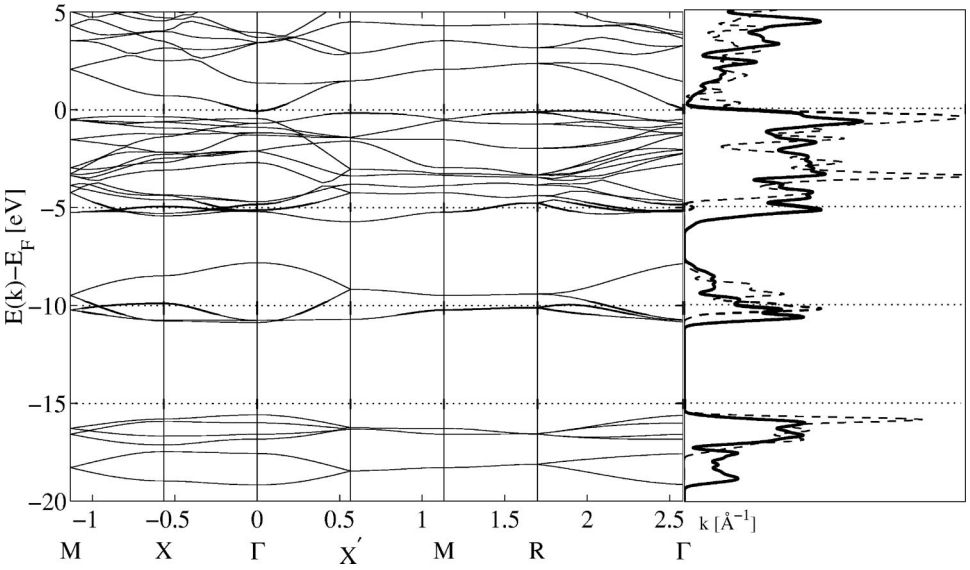

FIG. 4. The band structure and DOS for δ-Bi_2O_3. In the DOS panel, the solid and dashed lines correspond to the $\langle 100 \rangle$- and $\langle 111 \rangle$-vacancy structures, respectively.

The band structure for the δ phase has more dispersion compared to the α phase and the band gap between the valence and conduction bands is virtually absent. The highest occupied valence state between the Γ and R points has an energy of 20 meV above the bottom of the conduction band at the Γ point. This results in some states being occupied at the bottom of the conduction band although the energy gap at the Γ point was 0.37 eV. There is consequently a finite density of states at the Fermi level, resulting in semimetallic character for the δ phase. Under estimation of the band gap is a common problem in DFT calculations related to the self-interaction between the electron and its contribution to the electron density.[41] Medvedeva *et al.*,[22] who found the δ phase to be metallic, used a self-interaction correction in their calculations which did not alter the magnitude of the band gap significantly. Conductivity measurements for thin films of δ-Bi_2O_3 have also revealed a finite density of states at the Fermi level. This indicates that the band gap for the δ phase can be much smaller than for the α phase.

C. Zn doping in the α and δ phases of Bi_2O_3

The mixing of ZnO and Bi_2O_3 is not a favorable process according to the phase diagram by Peigney and Rousset.[42] Only very limited amounts of Zn can be incorporated into Bi_2O_3 and the mixing would result in a phase separation between ZnO and a bismuth-rich oxide compound $ZnBi_{38}O_{60}$. There have also been reports of the formation of $ZnBi_2O_6$ having a trirutile structure using hydrothermal synthesis.[43]

We have investigated the substitution process where a Bi atom in Bi_2O_3 is replaced by a Zn atom in order to determine the equilibrium concentration of Zn in the α and δ phases of Bi_2O_3. The impurity-induced effects on the electronic structure have also been studied to see if any active impurity states are formed in the band gap region.

The expression for the impurity concentration in Eq. (1) is based on the assumption that the formation energy is independent of the impurity concentration. However, in supercell calculations there is a problem in that the impurity could be interacting with itself due to the periodic boundary conditions.[44] We have therefore studied the Zn substitution at various doping concentrations without relaxation to estimate the character and magnitude of the Zn-Zn interaction between nearest-neighboring Zn atoms in the α and δ phases of Bi_2O_3.

The formation energy under oxygen-rich conditions ($\mu_O = \mu_O^{O_2}$), presented in Fig. 5, decreased slightly as the Zn concentration was reduced. The variation in formation energy for the α phase was small, indicating that the Zn-Zn interaction was limited. The small fluctuation in formation energy for the α phase was probably due to the fact that nonequivalent Bi sites were populated as the concentration was varied. The difference in formation energy for substitu-

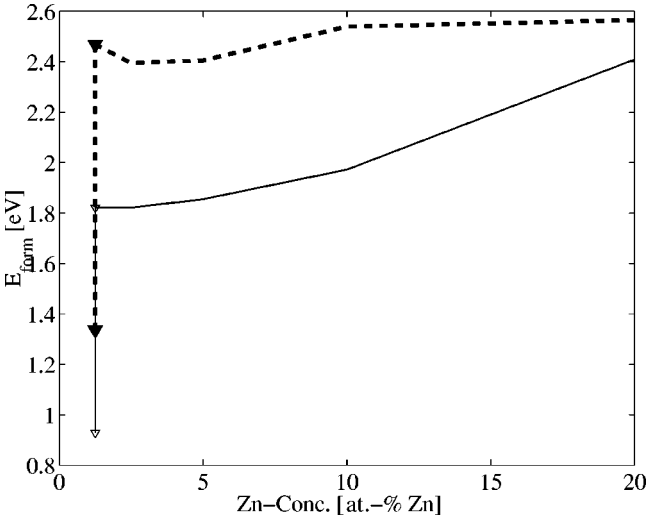

FIG. 5. The formation energy per Zn atom under oxygen-rich conditions as a function of Zn concentration. The dashed and solid lines show the results for Zn substitution in the α and δ phases, respectively. The vertical arrows indicate the relaxation energy at 1.25 at. % Zn. This corresponds to the incorporation of 1 Zn atom in the 80-atom supercell.

tion at the two nonequivalent Bi sites in the unit cell was 80 meV which is 47% of the difference between the smallest and largest values of the formation energy in Fig. 5 (i.e., 170 meV at 20 at. % Zn).

The changes in formation energy were more pronounced for the δ phase where the formation energy decreased from 2.4 eV to 1.8 eV when the doping concentration was reduced from 20 to 1.25 at. % Zn. This indicates that the Zn-Zn interaction was repulsive but the small differences in the formation energies further indicated that the magnitude of this interaction was not large. Figure 5 also shows that the formation energy plateaus at a Zn concentration of 1.25 at. % for the δ phase. This value was therefore chosen as the model concentration for studying the effect of an isolated Zn impurity in both the α and δ phases of Bi_2O_3.

The relaxation of the atoms in the Zn-doped Bi_2O_3 compressed the lattice around the Zn impurity for both phases. The nearest-neighboring Zn-O distance in the α phase decreased down to 1.9, 1.9, and 2.0 Å for the three nearest-neighboring O atoms. The relaxation energy for the Zn-doped α phase is indicated in Fig. 5 by the dashed arrow at 1.25 at. % Zn concentration. The relaxation of the Zn doped δ phase was more cumbersome than in the α phase because of a tendency to disrupt the crystal structure as discussed in the next section. The crystal structure could be maintained if the relaxation was restricted by freezing planes of atoms in the cell to limit the extent of the atomic displacements. In this case the Zn-O distance for the three nearest-neighboring O atoms in the δ phase decreased to 1.9, 2.1, and 2.1 Å. The corresponding relaxation energy is indicated in Fig. 5 by the thin arrow at 1.25 at. % Zn. The compression of the lattice around the Zn impurity was expected since the equilibrium Zn-O bond length in ZnO (2.0 Å) is shorter than the Bi-O bond length in Bi_2O_3 (2.2–2.6 Å in the α phase and 2.1–2.2 Å in the δ phase).

The most important impurity-induced effect on the electronic structure of the α phase was that the Zn substitution altered the number of valence electrons in the system. The Bi atom has three $6p$ electrons while the Zn atom has two $4s$ electrons in the valence configuration. The substitution consequently left the highest occupied band half filled in the Zn-doped system. This band had slightly smaller dispersion compared to the highest occupied valence band in the pure α phase with no minima at the Γ point. The highest fully occupied valence band on the other hand had a minimum at the Γ point, leading to the conclusion that this was the highest occupied valence band and that the half filled band was a Zn-induced acceptor state. The wave function for the acceptor state had significant d character originating from the Zn atom and it overlapped with the O atoms in the supercell. No clear localization could be observed around the impurity atom due to the limited size of the supercell. The amplitude of the wave function, on the other hand, varied throughout the supercell in contrast to the wave function of the highest occupied valence band in the pure α phase which had the same amplitude on every O atom in the supercell. The excitation energy from the top of the valence band to the acceptor level varied with Zn concentration. The excitation energy decreased from 230 meV at 5 at. % Zn down to 70 meV at 1.25 at. % Zn. This shift is probably caused by the repulsive Zn-Zn interaction which pushes the energy level of the acceptor state further into the band gap at higher doping levels.

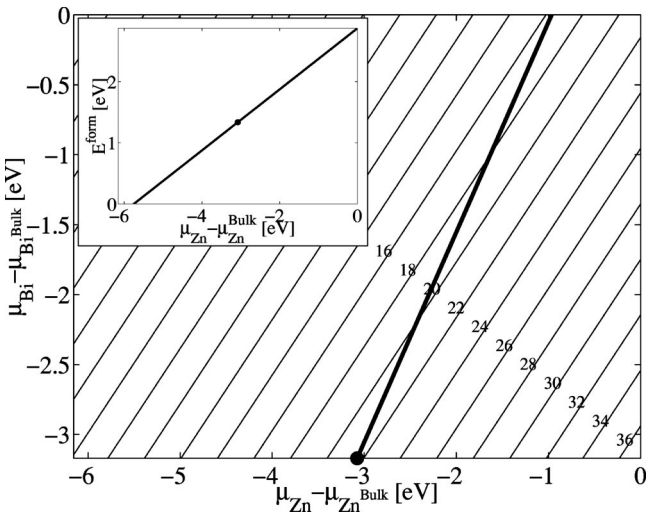

FIG. 6. A logarithmic contour plot of the Zn concentration in α-Bi_2O_3 at $T=1000$ K. The contour lines are labeled from $\log(C_i)=-8$ in the upper left-hand corner to 36 in the lower right-hand corner. The chemical potentials of Zn and Bi are given with respect to the bulk metal values and the lower limits on the plot are $2\Delta H_{ZnO}$ and $\Delta H_{Bi_2O_3}/2$ for Zn and Bi. The thick line is the ZnO limiting line for the Zn reservoir and the maximum concentration indicated by the bold circle is located at the intersect between the ZnO line and the minimum chemical potential for Bi. The inset shows the variation of the formation energy E_{form} along the ZnO line with the value at the maximum concentration indicated by a dot.

Figure 6 shows the equilibrium Zn concentration in the α phase of Bi_2O_3 obtained by inserting the results from the DFT calculations into the set of equations (1) and (2). These equations were solved at $T=1000$ K which is just below the α-δ phase transition temperature. It is seen that the Zn concentration increases when the Bi chemical potential decreases which means that the removal of Bi atoms becomes more favorable. The Zn concentration also increases when the Zn chemical potential increases which means that the reservoir for the Zn atoms becomes less energetically favorable relative to the substitution sites in Bi_2O_3. The formation of ZnO in the system is, however, setting an upper limit for μ_{Zn} indicated by the thick line in Fig. 6. The region to the right of the ZnO line is inaccessible since in this region μ_{Zn} is higher than the value in ZnO. In this case a separate ZnO phase would be formed instead of the solid solution. The formation energy along the ZnO line is shown in the inset to Fig. 6. It is seen to increase as μ_{Zn} increases because along this line 1.5 Zn atoms are exchanged for every Bi atom since three O atoms are needed to form the Bi_2O_3 molecule. The maximum Zn concentration, indicated by the bold circle in Fig. 6, occurs in the oxygen-rich limit where $\mu_O=\mu_O^{O_2}$ and the chemical potentials for Zn and Bi have the limiting values

$$\mu_{Zn}=\mu_{Zn}^{bulk}+\Delta H_{ZnO}$$

TABLE V. The quantities, defined in the text, used to calculate the equilibrium concentration of Zn in the α and δ phases of Bi_2O_3.

Phase	T [K]	E_{form} [eV]	N_s [atom/m^3]	C_i [atom/m^3]
α-Bi_2O_3	1000	1.34	2.39×10^{28}	4.22×10^{21}
δ-Bi_2O_3	1090	0.93	2.34×10^{28}	1.17×10^{24}

and

$$\mu_{Bi}=\mu_{Bi}^{bulk}+\frac{\Delta H_{Bi_2O_3}}{2}.$$

The formation energy for the Zn impurity at a substitution site in α-Bi_2O_3 was 1.34 eV and this corresponded to a concentration of 7.1×10^{-6} at. % Zn at $T=1000$ K.

The Zn concentration in the δ phase was studied at $T=1090$ K which is just below the melting point. The behavior for the δ phase was similar to the α phase but the formation energy of the Zn impurity was lower (0.93 eV) and consequently the equilibrium concentration was higher (2.0×10^{-3} at. % Zn). The values for the formation energy, equilibrium concentration, and Fermi level in the Zn-doped α and δ phases are summarized in Table V.

V. DISCUSSION

The good agreement between the calculated and experimental lattice parameters and atomic positions shown in Tables I and II for the α phase was expected since DFT calculations usually predict ground-state structural properties with high accuracy. The correspondence between the peaks in the DOS and the photoemission spectra for the valence band together with the size of the band gap provides further indication that we have an appropriate method to describe the low-temperature phase of Bi_2O_3.

The situation is more complicated for the high-temperature δ phase which can be considered to be in a supercooled state in our $T=0$ K calculation. The $\langle111\rangle$-ordered vacancy structure has been proposed based on symmetry arguments,[11] electrostatic arguments,[45] and from the results of LMTO calculations.[22] Our calculations, on the other hand, suggest that $\langle100\rangle$-vacancy ordering would be more favorable. We have therefore analyzed the different energy contributions to the total energy in order to understand why this is. Table VI reveals that the ion-ion and electron-electron interaction terms favored the symmetric $\langle111\rangle$ configuration but this effect was overcompensated by the electron-ion interaction. This suggests that the δ phase is gaining energy by accumulating a higher electron density close to the ion cores which increases the electron-ion interaction. This accumulation of electron density depends on the local atomic environment. Figure 4, which compares the DOS for the $\langle100\rangle$- and $\langle111\rangle$-vacancy structures, shows that O atoms with six O neighbors have a lower energy than O atoms with four O neighbors. This supports the idea that the gain in electron-ion energy for atoms surrounded by a higher number of neighbors, as in the $\langle100\rangle$-vacancy structure, dominates over the effect of lower symmetry which increases the ion-ion and electron-electron interaction energies. The final preference for the $\langle100\rangle$-vacancy structure over the $\langle110\rangle$ orientation is determined by the kinetic energy which is lower for the $\langle100\rangle$ compared to the $\langle110\rangle$ orientation.

TABLE VI. The different contributions to the total energy of δ-Bi_2O_3. The values are given relative to the α phase which is considered as the ground state. The terms are kinetic energy E_{kin}, ion-ion interaction energy $E_{I\text{-}I}$, electron-ion interaction energy $E_{I\text{-}e}$ (including local and nonlocal terms in the pseudopotential), electron-electron interaction energy E_H and E_{xc}, a correction term for the use of pseudopotentials E_{psc}, and the total energy E_{tot}.

Phase	E_{kin} [eV]	$E_{I\text{-}I}$ [eV]	$E_{I\text{-}e}$ [eV]	E_H [eV]	E_{xc} [eV]	E_{psc} [eV]	E_{tot} [eV]
δ-$\langle111\rangle$	−2.50	15.43	−15.90	7.87	1.93	−4.94	1.88
δ-$\langle110\rangle$	1.58	78.90	−153.76	77.60	−0.07	−3.27	0.97
δ-$\langle100\rangle$	0.81	110.24	−215.24	108.27	0.05	−3.32	0.80

The difference in heat of formation, ΔH, between the $\langle110\rangle$- and $\langle100\rangle$-ordered vacancy structures was 0.17 eV/(Bi_2O_3 molecule), which is approximately twice the sum of the numerical uncertainty in the basis set and k-point sampling, suggesting that the numerical precision is sufficient to distinguish between the $\langle110\rangle$ and $\langle100\rangle$ ordering. We have, in addition, compared the three vacancy orientations using the PZ-LDA (Ref. 41), exchange-correlation functional and also used the CASTEP code[46] to determine whether LDA or another DFT code gives the same ordering. Both the LDA and CASTEP calculations reproduced the ordering which favored the $\langle100\rangle$ vacancy orientation. This shows that calculations using LDA or GGA exchange-correlation functionals and pseudopotentials unambiguously favor the $\langle100\rangle$ vacancy orientation. The finite-temperature effects are harder to determine with our treatment. The thermal energy at the $\delta\rightarrow\alpha$ phase transition temperature $T_{\delta\rightarrow\alpha}=1003$ K is $k_BT_{\delta\rightarrow\alpha}\approx86$ meV or approximately half the difference in ΔH between the $\langle110\rangle$- and $\langle100\rangle$-vacancy structures. Figure 3 also shows that there are significant barriers to overcome for the δ phase to complete a full transition between the $\langle100\rangle$- and $\langle110\rangle$-vacancy configurations. These results imply that the $\langle100\rangle$-vacancy ordering is the most favorable configuration for the δ phase.

In order to investigate the stability of $\langle100\rangle$-vacancy ordering against the formation of local $\langle110\rangle$- or $\langle111\rangle$-vacancy regions, we have calculated the formation energy for a ''displaced'' vacancy in the $\langle100\rangle$ structure. The displaced vacancy is a unit cell where the vacancy orientation deviates from the regular vacancy ordering in the oxygen sublattice, for instance a $\langle110\rangle$-vacancy unit cell in an otherwise $\langle100\rangle$-vacancy lattice. We have considered a displaced vacancy concentration of 12.5% by changing the vacancy orientation in one of the eight unit cells in the [100] supercell as shown schematically in Fig. 7. In this case the formation energy of the displaced vacancy is the difference in vacancy formation energy between two defect orientations in a cell containing the same number of atoms. The formation energy in Eq. (2) then reduces to the difference in total

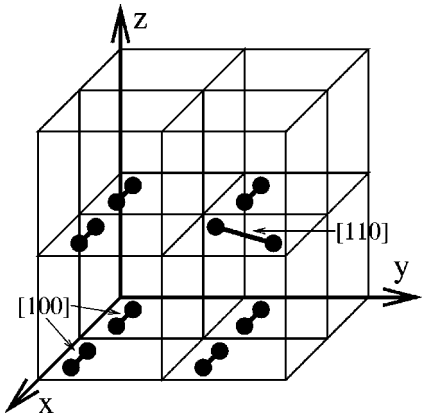

FIG. 7. A schematic diagram of a displaced [110] vacancy in an otherwise [100]-ordered δ phase. The bold circles indicate the pairs of vacancies along the two different orientations.

energy between the ideal defect orientation and the supercell containing the displaced defect, $E_{form}(\langle 110\rangle) = E(\langle 100\rangle,\langle 110\rangle) - E(\langle 100\rangle)$. We have also studied the effect of different orientations of the same type of vacancy ordering by considering a [010] vacancy in an otherwise [100] ordered structure and a zigzag chain of $\langle 111\rangle$ vacancies compared to a [111]-ordered cell.

Disturbing the [100]-vacancy orientation in the oxygen sublattice by displacing a vacancy rigidly, without relaxation, was not energetically favorable. The formation energy of a local [110] vacancy was 1.1 eV and the corresponding formation energy for a local [010] or a [111] vacancy was 1.5 eV and 3.1 eV, respectively. A zigzag chain of $\langle 111\rangle$ vacancies, on the other hand, had a lower energy than the regular [111]-ordered structure and this decreased the energy difference between the $\langle 100\rangle$ and $\langle 111\rangle$ structures to 0.65 eV per Bi_2O_3 molecule.

The formation of displaced vacancies imposed strong forces on the surrounding atoms and releasing them to allow relaxation had dramatic effects on the structure. A Bi atom in the fluorite structure has six nearest-neighbor O atoms with an ideal Bi-O bond distance of $a_0\sqrt{3}/4 \approx 2.4$ Å. However, relaxation of the displaced vacancy structures moved most of the Bi and O atoms closer together. The new neighbor distances varied between 2.1 and 2.5 Å. This distribution of Bi-O bond distances is similar to that found in the α phase which suggests that if the δ-phase system is perturbed sufficiently, it could transform into a structure at least resembling the α phase. In addition, the relaxation energy was found to be very large. Although we did not pursue the relaxation until an equilibrium structure was obtained, the difference in heat of formation between the α and δ phases diminished significantly from an initial value of 0.78 eV/(Bi_2O_3 molecule) to 0.32 eV/(Bi_2O_3 molecule). We interrupted the relaxation at this point even though the ionic forces were not negligible because the system was not apparently approaching an equilibrium structure. To properly simulate a $\delta \rightarrow \alpha$ phase transformation would require a change in shape of the supercell during relaxation which, unfortunately, is not a feature currently implemented in the computer code. Our results are therefore suggestive rather than conclusive. However, the possible tendency for a phase transformation from a high-temperature phase to a low-temperature phase is not surprising since the calculations did not include finite-temperature effects. In the $T=0$ K formalism, the δ phase must be viewed as a supercooled state, but if there are large enough structural disturbances, then these could trigger a phase transformation. Interestingly, the incorporation of a Zn substitutional impurity into the δ phase was apparently sufficient to destabilize the crystal structure. A full relaxation of the supercell containing an impurity atom led to a disruption of the crystal structure. This resulted in an unphysical negative formation energy of the order -8 eV for the Zn impurity, when the perfect $\langle 100\rangle$-ordered δ phase was taken as reference system in Eq. (2). Treating defects in the δ phase using the $T=0$ K formalism is obviously a very delicate matter which requires large supercells and freezing atoms in order to maintain the crystal structure of the high-temperature phase.

Since the stability of the δ phase is sensitive to perturbations in structure, our discussion of the solubility of Zn in Bi_2O_3 is restricted to substitution in the α phase. The maximum Zn concentration was computed to be 7.1×10^{-6} at. % Zn at $T=1000$ K (i.e., only one Zn atom per 5.7×10^9 Bi atoms). This low solubility is probably connected to the different electronic structures of Zn and Bi. The Bi atom has a larger number of valence electrons whose wave functions have a different character and larger radius than in the Zn atom. This is reflected in the higher atomic coordination of Bi in Bi_2O_3 compared to Zn in ZnO. The Zn atom does not, therefore, find a suitable substitution environment in Bi_2O_3 even after relaxation and the resulting formation energy is high. Our previous calculations[10] have similarly shown that Bi substitution in bulk ZnO is energetically unfavorable and that there is a significant segregation energy for a Bi atom residing in the $\Sigma=13$ tilt grain boundary. This suggests that the mechanical mixing of ZnO and Bi_2O_3 to form a single-solution phase having either a wurtzite or a monoclinic structure is not favorable. The mixture of ZnO and Bi_2O_3 would phase separate and evidence for this is provided by x-ray diffraction experiments[47] on sintered ZnO-Bi_2O_3 powders of varying Bi content which have shown that bismuth forms thin layers of β-Bi_2O_3 on the surface of the ZnO grains. The formation of bismuth-rich oxides at triple junctions in polycrystalline varistor materials is another example of phase separation between ZnO and Bi_2O_3.[6,7] There is, however, evidence that a single-solution phase of a different structure can be fabricated by hydrothermal synthesis to form $ZnBi_2O_6$ which has a trirutile structure.[43] In general, though, the low computed solubility for Zn in the α phase of Bi_2O_3 is consistent with the experimental observation of phase separation between ZnO and Bi_2O_3.

VI. CONCLUSIONS

We have investigated the atomic and electronic structure of the pure and Zn-doped α and δ phases of Bi_2O_3 by *first-principles* calculations. The lattice parameters and atomic positions for the α phase were in good agreement with experimental measurements. The calculated DOS corresponded

very closely to photoemission spectra for the valence band but the peaks for the semicore electrons were slightly shifted towards higher energy. We attribute this shift to the use of pseudopotentials in our calculations. The optical band gap of 2.6 eV was also in good agreement with experimental values. Based on these results we conclude that our total energy method is able to give a reliable description of the structural and chemical properties of Bi_2O_3.

Our calculations on the δ phase showed that the $\langle 100 \rangle$-ordered vacancy structure was energetically the most favored in contrast to previous LMTO studies. Further investigations of the stability of the δ phase against the spontaneous formation of regions of different vacancy orientations suggested that the structure could be destabilized by small perturbations. The δ phase should, however, be considered as a supercooled phase in our calculations since it is a high-temperature phase which would transform into the α phase at $T=1003$ K. The relaxation of the supercells containing either a displaced vacancy or a Zn impurity led to a disruption of the ordered fluorite structure suggesting a tendency for phase transformation into the α phase.

We have also investigated substitutional Zn doping of Bi_2O_3 and found that the formation energy for a Zn impurity in the α phase was 1.34 eV, giving an equilibrium concentration of 7.1×10^{-6} at. % Zn at $T=1000$ K. The low solubility for Zn in the α phase of Bi_2O_3 is consistent with the phase separation between ZnO and Bi_2O_3 observed in varistor materials.

ACKNOWLEDGMENTS

J.C. has been supported by the Swedish Natural Science Research Council and H.S.D. acknowledges Grant No. PRAXIS XXI/BD/13944/97. The calculations were performed using the UNICC resources at Chalmers, Gothenburg, Sweden.

*Electronic address: johanc@fy. chalmers. se

[1] N.R. Khasanova, A. Yamamoto, S. Tajima, X.-J. Wu, and K. Tanabe, Physica C **305**, 275 (1998).
[2] R.J. Cava, B. Batlogg, J.J. Krajewski, R.C. Farrow, L.W. Rupp, Jr., A.E. White, K.T. Short, W.F. Peck, Jr., and Y. Kometani, Nature (London) **332**, 814 (1988).
[3] T. Takahashi and H. Iwahara, Mater. Res. Bull. **13**, 1447 (1978).
[4] D.R. Clarke, J. Am. Ceram. Soc. **82**, 485 (1999).
[5] M. Matsuoka, Jpn. J. Appl. Phys. **10**, 736 (1971).
[6] E. Olsson and G. Dunlop, J. Appl. Phys. **66**, 4317 (1989).
[7] M. Elfwing, R. Österlund, and E. Olsson, J. Am. Ceram. Soc. **83**, 2311 (2000).
[8] J.R. Lee, Y.M. Chiang, and G. Ceder, Acta Mater. **45**, 1247 (1997).
[9] D.R. Clarke, J. Appl. Phys. **49**, 2407 (1978).
[10] J.M. Carlsson, H.S. Domingos, B. Hellsing, and P.D. Bristowe, Interface Sci. **9**, 143 (2001).
[11] L.G. Sillén, Ark. Kemi, Mineral. Geol. **12A**, 1 (1937).
[12] R. Evarestov, V. Shapovalov, and V. Veryazov, Phys. Status Solidi B **183**, K15 (1994).
[13] H.A. Harwig, Z. Anorg. Allg. Chem. **444**, 151 (1978).
[14] J.W. Medernach and R.L. Snyder, J. Am. Ceram. Soc. **61**, 494 (1978).
[15] T.P. Debies and J.W. Rabalais, Chem. Phys. **20**, 277 (1977).
[16] F. Rogemond, C. Pedrini, and H. Chermette, Chem. Phys. **146**, 129 (1990).
[17] R. Evarestov, V. Shapovalov, and V. Veryazov, Phys. Status Solidi A **183**, K15 (1994).
[18] V.P. Zhukov, V.M. Zhukovskii, V.M. Zainullina, and N.I. Medvedeva, J. Struct. Chem. **40**, 831 (1999).
[19] G. Gattow and H. Schröder, Z. Anorg. Allg. Chem. **318**, 176 (1962).
[20] P.D. Battle, C.R. Catlow, J. Drennan, and A.D. Murray, J. Phys. C **16**, L561 (1983).
[21] P.D. Battle, C.R. Catlow, J.W. Heap, and L.M. Moroney, J. Solid State Chem. **63**, 8 (1986).
[22] N. Medvedeva, V.P. Zhukov, V. Gubanova, D. Novikov, and B. Klein, J. Phys. Chem. Solids **57**, 1243 (1996).
[23] P. Jacobs and D. MacDonaill, Solid State Ionics **18**, 209 (1986).
[24] P. Jacobs and D. MacDonaill, Solid State Ionics **23**, 279 (1987).
[25] S. Boyapati, E. Wachsman, and N. Jiang, Solid State Ionics **140**, 149 (2001).
[26] Y. Vidadi, Y. Guseinov, V. Bagiev, and T. Rafiev, Physica B **173**, 415 (1991).
[27] T. Atou, H. Faqir, M. Kikuchi, H. Chiba, and Y. Syono, Mater. Res. Bull. **33**, 289 (1998).
[28] C. Chouinard and S. Desgreniers, Solid State Commun. **113**, 125 (2000).
[29] B. Hammer *et al.*, computer code DACAPO-1.30, Center for Atomic Scale and Materials Physics, Danmarks Tekniske Universitet, Lyngby, Denmark (1998).
[30] P. Hohenberg and W. Kohn, Phys. Rev. **136**, B864 (1964).
[31] W. Kohn and L.J. Sham, Phys. Rev. **140**, A1133 (1965).
[32] J.P. Perdew, J.A. Chevary, S.H. Vosko, K.A. Jackson, M.R. Pederson, D.J. Singh, and C. Fiolhais, Phys. Rev. B **46**, 6671 (1992).
[33] D. Vanderbilt, Phys. Rev. B **41**, 7892 (1990).
[34] H.J. Monkhorst and J.D. Pack, Phys. Rev. B **13**, 5188 (1976).
[35] M.J. Gillan, J. Phys.: Condens. Matter **1**, 689 (1989).
[36] S.B. Zhang and J.E. Northrup, Phys. Rev. Lett. **67**, 2339 (1991).
[37] C.G. Van de Walle, D.B. Laks, G.F. Neumark, and S.T. Pantelides, Phys. Rev. B **47**, 9425 (1993).
[38] Y. Yourdshahyan, C. Ruberto, L. Bengtsson, and B.I. Lundqvist, Phys. Rev. B **56**, 8553 (1997).
[39] P. Schröer, P. Krüger, and J. Pollmann, Phys. Rev. B **47**, 6971 (1993).
[40] D. Vogel, P. Krüger, and J. Pollmann, Phys. Rev. B **54**, 5495 (1996).
[41] J.P. Perdew and A. Zunger, Phys. Rev. B **23**, 5048 (1981).
[42] A. Peigney and A. Rousset, J. Am. Ceram. Soc. **79**, 2113 (1996).
[43] N. Kumada, N. Takahashi, N. Kinomura, and A.W. Sleight, Mater. Res. Bull. **32**, 1003 (1997).
[44] G. Makov and M.C. Payne, Phys. Rev. B **51**, 4014 (1995).
[45] H.A. Harwig and J.W. Weenk, Z. Anorg. Allg. Chem. **444**, 167 (1978).
[46] M.C. Payne, M.P. Teter, D.C. Allan, T.A. Arias, and J.D. Joannopoulos, Rev. Mod. Phys. **64**, 1045 (1992).
[47] L. Benes, V. Rambousek, M. Predota, and J. Horak, J. Mater. Sci. **21**, 3345 (1986).